Acta Geochimica
2022, Volume 41, Pages 12-23
https://doi.org/10.1007/s11631-021-00513-y
https://archimer.ifremer.fr/doc/00746/85826/

Pure forsterite in Nyiragongo lavas: evidence for subsolidus oxidation of volcanic rocks

Badriyo Agama Innocent [1, 3], Chazot Gilles [2, *], Kamgang Pierre [1]

[1] Département Des Sciences de la Terre, Faculté Des Sciences, Université de Yaoundé I, B.P. 812, Yaoundé, Cameroon
[2] Laboratoire Géosciences Océan, Institut Universitaire Européen de la Mer, Université de Brest (UBO), UMR 6538, Place Copernic, 29280, Plouzané, France
[3] Observatoire Volcanologique de Goma, B.P. 484, Goma, Nord-Kivu, Democratic Republic of the Congo

* Corresponding author : Innocent Badriyo Agama, email address : Gilles.Chazot@univ-brest.fr

Abstract :

Some volcanic rocks from Nyiragongo volcano in the Democratic Republic of Congo contain highly oxidized olivine crystals. These olivines crystals are made of two phases, dark olivine on backscattered electron images of pure forsterite composition and grey Mg-poor areas made of olivine and iron-rich oxides. Calculation of the initial composition confirms that they are primary olivine with late separation of two different olivine compositions. Pure forsterite is enriched in SiO2 but contains lower amounts of CaO than Fe-rich areas, in agreement with expected partitioning of these elements related to the composition of the olivine. Iron-rich oxides formed around or inside the olivine crystals during the separation process and confirm a highly oxidized environment during their evolution. We propose that this separation occurred during subsolidus recrystallization under high fO2 conditions of the olivine crystals after cooling of the volcanic rocks. It provides evidences for circulation of iron-rich fluids or gas inducing deuteritic processes occurring in the large volcanic cone of the Nyiragongo, in relation with the presence of a shallow magma chamber connected to a large and permanent lava lake

Keywords : Nyiragongo, Olivine, Forsterite, Oxidation

1. Introduction

The Nyiragongo volcano, located in the Democratic Republic of Congo is one of the eight volcanoes of the Virunga Volcanic Province (VVP), which is part of the western branch of the

East African Rift System. Continental extension and related magmatism in that area started at ca 38 Ma in Ethiopia and has subsequently extended southward into Kenya and Northern Tanzania (Dawson 2012; Jung et al. 2019). The Virunga Volcanic Province is characterized by unusual silica-undersaturated, ultra-alkaline volcanism that started erupting ~ 11 Ma ago and which is still active today in Nyiragongo and Nyamuragira volcanoes (Pouclet and Bram 2021).

Nyiragongo volcano is a large cone culminating at 3470 m a.s.l, with a large crater at the top, in which a semi-permanent lava lake is present. The Nyiragongo lavas are foiditites (Le Bas et al. 1986) highly silica undersaturated and belong to the leucite-bearing nephelinite series. The volcano produces highly porphyritic lavas. Phenocrysts are various type of feldspathoïds (leucite, nepheline), melilite, clinopyroxene and olivine. We analyse olivine phenocrysts and microlites in many melilitite, nephelinite and basanite samples from Nyiragongo volcano. Their composition can be very Mg-rich in the basanites, with up to 90% forsterite component in some samples. Olivine is more iron-rich in nephelinites, with compositions down to Fo_{52} (Badriyo Agama, PhD thesis unpublished data).

As a whole, olivines in Nyiragongo lavas contain between 0.05 and 0.4 wt.% NiO, but can be very Ca-rich, from 0.5 wt.% CaO in basanites up to 1.5% CaO in nephelinites. Highest values of CaO often occur at the rim of large phenocrysts, but the core of some phenocrysts can also be Ca-rich.

In a few samples, olivine phenocrysts appear heterogenous and oxidized under the microscope. It appears that these crystals are made of two contrasted kinds of areas with different chemical compositions. We focussed on these olivine crystals in two selected samples in order to better understand the mechanisms leading to this phenomena.

2. Samples

From a large set of volcanic rocks coming from a recent field works on the South flank of the Nyiragongo volcano, two samples containing oxidized olivine phenocrysts were selected for analyses. AND-3 come from the Andrade cone, on the South flank of the Nyiragongo volcano, South East of the Shaheru satellite volcano. MGR-2 was sampled on the Mugara volcanic scoria cone, also on the South flank of the volcano, but at lower altitude.

Sample AND-3 comes from a dyke. The volcanic rock looks oxidized, with a reddish colour. It has a microlitic texture with few clinopyroxene phenocrysts and more abundant microphenocrysts of clinopyroxene and olivine. The sample contains many vacuoles of irregular shape. A flow banding is clearly visible on hand-specimen and under the microscope, and is associated with more glassy parts. Olivine is only present as microphenocrysts, and all the crystals are highly oxidized and show two different kinds of composition.

Sample MGR-2 is a volcanic bomb from a scoria cone. It is a massive lava with a reddish colour. The rock has a microlitic texture with few clinopyroxene phenocrysts. Microlites are made of clinopyroxene and felspathoïds (nepheline) disseminated in a dark groundmass with many small vacuoles. Olivine is present as microphenocrysts, and as for AND-3, all the crystals are strongly oxidized.

3. Olivine description

In the two studied samples, all the olivine crystals are oxidized and their shape and organization can only be observed in reflected light or using backscattered electrons (BSE) with the electron microprobe. All the crystals have the same internal structure, with large BSE-dark parts, separated by elongated, not always parallel, BSE-grey zones (Fig. 1). In many crystals, the BSE-grey parts are more regularly organized close to the rim than in the center of the grains. Many crystals are rimed by a heterogeneous light-grey zone, a few tens of micrometers large,

containing many backscatter bright white minerals. In MGR-2 sample, the central part of the BSE-grey zones also sometimes contains small backscatter bright minerals (Fig. 1A).

4. Analytical techniques

Major element composition of minerals was measured using an electron microprobe (Microsonde Ouest, CAMECA SX100) at the Laboratoire Géosciences Océan (University of Brest, France) on C-coated polished thin sections. Mineral analyses were performed with operating conditions of 15 kV and 20 nA, 10 s counting time on the peak and a spot size of 1 µm. Compositional maps and Back Scattered Electron (BSE) images were acquired on the same microprobe.

The $\phi(\rho Z)$ matrix correction was applied based on Pouchou and Pichoir (1988). Standards (element, emission line) are: albite (Na Kα, Si Kα), InP (P Kα), forsterite (Mg Kα), corundum (Al Kα), orthoclase (K Kα), wollastonite (Ca Kα), synthetic manganese titanate (Mn Kα, Ti Kα), pure iron (Fe Kα).

Whole-rock major and some trace elements were measured on the Horiba - Jobin-Yvon® Ultima 2 ICP-AES at the IUEM (European Institute for Marine Studies, Pôle de Spectrométrie Océan, Brest, France). A description of the analytical procedure is given in Cotten et al. (1995). Elements were determined from an H_3BO_3 solution, boron being used as internal standard for ICP-AES analysis. For major elements, relative standard deviation is 1% for SiO_2 and 2% for the other major elements, except for low values (<0.50 wt. %), for which the absolute standard deviation is ±0.01 wt. %.

5. Results

AND-3 and MGR-2 rocks are basanites with SiO_2 ranging from 40.4 to 42.2 wt.% and MgO content ranging from 5.95 to 7.92 wt.% (Table 1). Similarly to other rocks from Nyiragongo volcano, they are highly silica-undersaturated and their CIPW normative composition contains between 12 and 17 % normative nepheline and between 12 and 18 % normative leucite.

We analysed the different parts of several olivine grains in the two samples AND-3 and MGR-2. The results are presented in Table 2 and were compared to olivine analyses we made in other samples from Nyiragongo volcano, similar to already published olivine analyses from this volcano. Our results, in agreement with olivine compositions from Nyiragongo nephelinites published by Platz et al. (2004) or Andersen et al. (2012) show that most olivine have chemical composition ranging from Fo_{70} to Fo_{90}. In the two studied samples, the BSE-dark part of olivine is always made of almost pure forsteritic olivine, with composition ranging from $Fo_{96.3}$ to $Fo_{99.7}$ (Fig. 2). The composition of the BSE-grey part is more variable, and, if considered as olivine, ranges from Fo_{56} to Fo_{61} in MGR-2 and from Fo_{27} to Fo_{72} in AND-3. Only one analysis in MGR-2 sample has a composition similar to normal Nyiragongo olivines, with Fo_{81}.

Oxide crystals have been analysed in the rims of several crystals. Oxides in volcanic rocks from Nyiragongo volcano are usually Ti-rich, belonging to the titanomagnetite series (Badriyo Agama, unpublished data). Oxides close to olivine grains in AND-3 and MGR-2 contain less than 7 wt.% TiO_2 (except for one analysis) and are Ti-poor titanomagnetite, close to the magnetite end-member (Table 4). Their composition is thus significantly different compared to oxides in Nyiragongo volcanic rocks (Platz et al.,, 2004; Andersen et al., 2012; Badriyo Agama, PhD thesis unpublished data). End-member calculations performed using the application published by Ferracutti et al. (2015) confirm that the analysed oxides are mostly magnetite-magnesioferrite, with small proportions of ulvospinel component.

6. Discussion

6.1 Composition of primary olivine

In order to understand the processes leading to these "two-phases" olivine crystals in some Nyiragongo volcanic rocks, it is important to know if we can have some information about the composition of the "primary" olivine before oxidation.

For the four olivine crystals presented in Fig. 1, we calculated the composition of the primary olivine, before separation in two phases with different forsteritic content, considering that the low-Mg BSE-grey parts are made of olivine. Using image-processing software, we produced colour images of the crystals, with one colour for the BSE-dark parts and another colour for the BSE-grey parts (Fig. 3). We excluded the rim of the crystals because electron microprobe analyses show that they are heterogeneous and made of oxides and different silicates, too small to be analysed. Counting the pixel number for each colour gave us the proportions of the two types of olivine. The results of these calculations are presented in the Table 3 and shown on the Fig. 4B. The proportions of BSE-dark and BSE-grey olivine are similar in the different crystals, with 66 to 77 % dark and 22 to 34% grey. The results of the calculation show that the primary olivines had compositions ranging from Fo_{85} to Fo_{91} and CaO content ranging from 0.24 to 0.30 wt.%. The high Fo values are similar to the most magnesian olivines from Nyiragongo volcano, and the calculated CaO values are close to the lowest values obtained in the Nyiragongo lavas (Fig. 2 and 4B). The results are broadly consistent with the formation of two different phases during a subsolidus event.

6.2 Partitioning of elements

As shown on the figure 2, olivine in Nyiragongo lavas has a composition ranging from Fo_{75} to Fo_{90}. Olivines in samples AND-3 and MGR-2 probably shared the same characteristics before their alteration, and the calculations of the primary olivines from the proportions of BSE-dark

and BSE-grey parts (Fig. 3) confirm these primary compositions between Fo_{80} and Fo_{90} in these samples. During alteration, chemical elements can incorporate preferentially in the Mg-rich olivine or in the Fe-rich phases. In volcanic olivine, SiO_2 is positively correlated to the Fo content, and olivine in Nyiragongo lavas follows the same trend as olivine worldwide (Fig. 4A). In AND-3 and MGR-2 samples, pure forsterite is enriched in silica, with up to 43.7 wt.% SiO_2. This value is in agreement with stoichiometric value calculated for pure forsterite and shown on the figure 4A. On the opposite, the Fe-rich phase is low in silica but lies above the trend for worldwide olivine. These analyses do not follow the trend for stoichiometric olivine (Fig. 4B). This can reflects the fact that the BSE-grey part of the crystals is made of a mixture of olivine associated with iron oxides crystallized during oxidation of the primary olivine, thus pushing the olivine composition above the stoichiometric trend. Microprobe analyses of the BSE-grey parts of olivine crystals can thus be a mixture of olivine and very small crystals of oxides, explaining the low sums of electron probe analyses for these parts of the crystals.

The calcium content of olivine crystallizing in mafic melts depends mostly upon the concentration of calcium and alkaline elements in the melt and is independent of pressure, temperature and oxygen fugacity below 20 kbar (Jurewizc and Watson 1988; Libourel 1999). Nyiragongo magmas are Ca-rich, many lavas contain between 14 and 19 wt.% CaO (Platz et al. 2004) and are also highly enriched in Na and K. Accordingly, olivine in Nyiragongo lavas is also Ca-rich, with CaO content up to 1.5 wt.%, well above the trend for worldwide olivine (Fig. 4B). In AND-3 and MGR-2 samples, pure forsterite parts contain lower CaO, always below 0.4 wt.% (except for 2 analyses). During two-phases separation, Ca is preferentially partitioned outside Mg-rich olivine, with content up to 1.3 wt.% CaO in the BSE-grey parts. This observation is consistent with experimental results showing that Ca incorporation in olivine is favoured by the activity of iron, and thus decreases when the Fo value of olivine increases (Jurewicz and Watson 1988).

168 *6.3 Distribution of chemical elements and oxide formation*

169 Chemical mapping was performed on a full olivine grain from MGR-2 (Fig. 5). The results
170 confirm and enhance the observations inferred from the in-situ chemical analyses of the
171 different part of the crystal. The BSE-dark part, made of pure forsterite do not contain any
172 detectable Ca (Fig. 5A) and Fe (Fig. 5B). The iron-rich part is clearly enriched in Ca, as the Ca
173 map shows the same distribution pattern visible on the BSE image (Fig. 1A). These patterns are
174 also well visible with the iron distribution, which is clearly not homogeneous and shows
175 increasing content towards the center of the iron-rich sectors (Fig. 5B). Mg distribution
176 confirms these observations, with high concentrations in the pure forsterite part of the crystal
177 and lower content in the Fe-rich parts (Fig. 5C). As noted for iron, there is a gradient in the Mg
178 content, with decreasing intensity towards the center of these Fe-rich parts. The silica
179 distribution is more homogeneous (Fig. 5D), but still shows slightly higher Si content in pure
180 forsterite, as observed from the chemical analyses (Fig. 4A).

181 On the BSE images (Fig. 1) the olivine crystals are rimed by a grey zone. At higher
182 magnification, this zone appears to be heterogeneous and made of different mineral phases, too
183 small to be analysed by the electron microprobe (Fig. 5A). It is rich in Ca, Fe and to a lesser
184 extend in Mg (Fig. 5) but very low in K. It is probably made of iron-oxides, clinopyroxene and
185 olivine. On the studied crystal in MGR-2, this zone is surrounded by a darker and larger area
186 connected to euhedral crystals of the same composition (Fig. 1). Very rich in K and Al, but with
187 no Fe, Ca and Na (Fig. 5), it appears to be pure kalsilite.

188 Occurrence of pure forsterite in volcanic rocks is rare and has been described in a few examples,
189 mostly from Iceland (Sigurdsson and Brown 1970), North Baikal region (Wenzel et al. 2002),
190 Stromboli volcano in Italy (Cortès et al. 2006) and the Big Pine Volcanic Field in California
191 (Blondes et al. 2012). In all these cases, the formation of forsteritic olivine is associated with a
192 highly oxidized environment, implying an oxidation event either in subliquidus or subsolidus

conditions. Haggerty and Baker (1967) showed that during high temperature deuteritic oxidation of olivine, pure fosterite is formed during breakdown of olivine crystals and expulsion of iron. They also demonstrated experimentally that this oxidation event can produce magnetite, hematite and enstatite associated to forsterite at atmospheric pressure, depending upon temperature and in the temperature range 600 – 1000°C.

According to these observations, magnetite, hematite and/or enstatite should be present in the Nyiragongo samples containing oxidized olivine. BSE images of some olivine crystals from MGR-2 and AND-3 samples (Fig. 1) confirm the presence of numerous oxides located all around the grains. Electron microprobe analyses show that these oxides are enriched in Fe^{3+}. Calculation of the end-members using the EMG application provided by Ferracutti et al. (2015) show that they belong to the magnetite-magnesioferrite series, with a low ulvöspinel component. They differ from the common oxides present as microlites and/or phenocrysts in Nyiragongo lavas which are titanomagnetite with ulvöspinel component ranging from 48 to 60% (Minisalle et al. 2019). As these magnetite-rich oxides are produced by olivine oxidation, they should also be present in association with the two different olivine compositions inside the olivine crystals. To check for these peculiar oxides, we produced high-resolution chemical maps of part of olivine crystal from both samples. In MGR-2, BSE image shows bright phases in the core of the low-Mg areas in olivine (Fig. 6A). On the chemical maps, these phases are iron-rich, with low Mg and no silica (Fig. 6B,C,D). They represent iron-rich oxides, probably magnetite of similar composition than the small grains surrounding the olivine crystals, but unfortunately too small to be analysed with the electron microprobe. This observation confirms that the BSE-grey parts of olivine crystals are a mixture of olivine and iron-rich oxides. Similar chemical maps have been obtained from part of an olivine crystal in AND-3. In this case, no bright iron-rich and silica-poor crystals are visible on the BSE and chemical maps (Fig. 7) while

some are present just outside the olivine crystal. In this case, it is possible that the resolution of the chemical maps is too low to be able to see these oxides is they are present.

6.4 Possible origin for the forsterite in olivine from Nyiragongo

Petrological observations as well as experimental works have related the occurrence of pure forsteritic olivine to highly oxidizing conditions. At Stromboli volcano, Cortès et al. (2006) argue for a subliquidus process, with forsterite crystallization related to degassing of the magmatic system associated with rapid decompression and increase in f_{O2}. Subliquidus forsterite cristallization is also advocated for Icelandic basalts, caused by magma-sea water interactions in the magma column (Sigurdsson and Brown 1970). At the opposite, forsterite in Big Pine basaltic flows formed in subsolidus conditions, during oxidations events occurring shortly after lava cooling (Blondes et al., 2012). Similar subsolidus or deuteritic conditions have been described and reproduced in experiments by Haggerty and Baker (1967) to explain the formation of forsteritic olivine accompanied by magnetite, hematite and/or enstatite formation.

In Nyiragongo lavas, the occurrence of forsterite associated with low-Mg mixture of olivine and iron-rich oxides in strongly oxidized lavas argue for a subsolidus formation of the forsterite, during a deuteritic process. This view is reinforced by the calculation of the primary olivine by combining the composition and proportions of forsteritic and low-Mg areas (Fig. 3) to obtain olivine with composition similar to those found in other rocks from this volcano, excepted for the iron content, enriched in the low-Mg parts of the crystals. This secondary oxidation process is confirmed by the global oxidation of the two studied samples, illustrated by their reddish colour.

Subsolidus recrystallization under high fo_2 conditions have been demonstrated in several cases, and has also been evidenced in Nyiragongo lavas. In their study of low-pressure fractionation trends of the Nyiragongo volcanic rocks, Platz et al. (2004) argued for the presence of large

241 amounts of CO_2 and H_2O allowing to the formation of abundant melilite. Nyiragongo magmas
242 are CO_2-rich, as confirmed by gas analyses (Sawyer et al. 2008) and by the presence of calcite
243 in the groundmass of many volcanic rocks (Andersen et al. 2012). The presence of large amount
244 of CO_2, either in magmas of fluids can increase the f_{O2} in great proportion, and has been
245 advocated to explain the formation of forsteritic olivine in skarns (Wenzel et al. 2002). In many
246 nephelinites from Nyiragongo, Andersen et al. (2012) observed static recrystallization of the
247 groundmass, with the formation of nepheline-kalsilite aggregates together with crystallization
248 of götzenite and combeite at temperature of ca. 600°C. They also show that post-magmatic
249 reequilibration of some samples has taken place at temperature below 600°C and in highly
250 oxidizing conditions, well above the QFM buffer (Andersen et al., 2014). As already proposed
251 by Sahama (1961, 1962), these low temperature crystallizations occurred in response to thermal
252 metamorphism and metasomatism from H_2O- and CO_2-bearing fluids. The presence of a
253 permanent lava lake connected with a shallow magma chamber at Nyiragongo volcano provides
254 a favourable environment for this process. The lava lake is continuously cooling, partly by
255 thermal conduction through the rocks of the lake walls. Fluctuations of the lava lake in the large
256 Nyiragongo crater allows episodic heating of the rocks in the large cone of the volcano. The
257 degassing magma provides large amounts of H_2O-CO_2 fluid or gas, probably enriched in iron
258 and which can percolate through the adjacent rocks and through the whole volcanic cone,
259 inducing metamorphism and/or metasomatism under high f_{O2} conditions.

260 This kind of highly oxidizing environment represents ideal conditions for the oxidation of
261 olivine crystals and formation of forsteritic olivine as well as iron-rich oxides. From these
262 observations, we can conclude that oxidized olivine in some Nyiragongo lavas accompanied by
263 the formation of pure forsterite associated to iron-rich oxides is one more evidence for deuteritic
264 processes occurring in the large volcanic cone of the Nyiragongo, in relation with the presence
265 of a shallow magma chamber connected to a large and permanent lava lake. Circulation of iron-

rich highly oxidizing fluids or gas induces a separation of olivines crystals into two components (pure forsterite and iron oxides). These observations confirm that thermal metamorphism and metasomatism car deeply modifiy and complexify the mineralogy of the already very special rocks of Nyiragongo volcano.

References

Andersen T, Elburg M, Erambert M (2012) Petrology of combeite- and götzenite-bearing nephelinite at Nyiragongo, Virunga Volcanic Province in the East African Rift. Lithos 152:105–121. doi: 10.1016/j.lithos.2012.04.018

Andersen T, Elburg M, Erambert M (2014) Extreme peralkalinity in delhayelite- and andremeyerite-bearing nephelinite from Nyiragongo volcano, East African Rift. Lithos 206-207:164–178. http://dx.doi.org/10.1016/j.lithos.2014.07.025

Blondes MS, Brando M.T, Reiners PW, Page FZ, Kita NT (2012) Generation of Forsteritic Olivine ($Fo_{99.8}$) by Subsolidux Oxidation in Basaltic Flows. J Petrol 53:971-984

Cortés JA, Wilson M, Condliffe E, Francalanci L (2006) The Occurrence of Forsterite and Highly Oxidizing Conditions in Basaltic Lavas from Stromboli Volcano, Italy. J Petrol 47:1345-1373

Cotten J, Le Dez A, Bau M, Caroff M, Maury RC, Dulski P, Brousse R. (1995) Origin of anomalous rare-earth element and yttrium enrichments in sub aerially exposed basalts: evidence from French Polynesia. Chem Geol119:115-138

Dawson JB (2012) Nephelinite-melilitite-carbonatite relationships: Evidence from Pleistocene-recent volcanism in northern Tanzania. Lithos 152:3–10

Ferracutti GR, Gargiulo MF, Ganuza ML, Bjerg EA Castro SM (2015) Determination of the spinel group end-members based on electron microprobe analyses. Mineral Petrol 109:153-160

Haggerty SE Baker I (1967) The Alteration of Olivine in Basaltic and Associated Lavas. Part I: High Temperature Alteration. Contrib Mineral Petrol 16:233-257

Jung SG, Choi S.H, Ji KH, Ryu JS Lee DC (2019) Geochemistry of volcanic rocks from Oldoinyo Lengai, Tanzania: Implications for mantle source lithology. Lithos 105223. doi: 10.1016/j.lithos.2019.105223

Jurewicz AJG Watson EB (1988) Cations in olivine, Part 1: Calcium partitioning and calcium-magnesium distribution between olivines and coexisting melts, with petrologic applications. Contrib Mineral Petrolo 99:176-185

Le Bas ML, Le Maitre R L, Streckeisen A, Zanettin B, IUGS Subcommission on the Systematics of Igneous Rocks (1986) A chemical classification of volcanic rocks based on the total alkali-silica diagram. J petrol 27:745-750

Libourel G (1999) Systematics of calcium partitioning between olivine and silicate melt: implications for melt structure and calcium content of magmatic olivines. Contrib Mineral Petrol 136:63-80

Minissale S, Zanetti A, Tedesco D, Morra V, Melluso L (2019) The petrology and geochemistry of Nyiragongo lavas of 2002, 2016, 1977 and 2017 AD, and the trace element partitioning between melilitite glass and melilite, nepheline, leucite, clinopyroxene, apatite, olivine and Fe-Ti oxides: a unique scenario. Lithos 332-333:296–311. doi: 10.1016/j.lithos.2019.02.023

Platz T, Foley SF Andre L (2004) Low-pressure fractionation of the Nyiragongo volcanic rocks, Virunga Province, D. R. Congo. J Volcanol Geotherm Res 136:269–295

310 Pouchou JL, Pichoir F (1988) A simplified version of the "PAP" model for matrix corrections
311 in EPMA. Microbeam analysis 315-318.

312 Pouclet A, Bram K (2021) Nyiragongo and Nyamuragira: e review of volcanic activity in the
313 Kivu rift, western branch of the East African Rift System. Bull Volc 83:10.
314 https://doi.org/10.1007/s00445-021-01435-6

315 Sahama G (1961) Thermal metamorphism of the volcanic rocks of Mt Nyiragongo (Eastern
316 Congo). Bull Com Géol Finl 196:151-174

317 Sahama TG (1962) Petrology of Mt. Nyiragongo: A Review. Trans Edinburgh Geolo Soc 19:1-
318 28

319 Sawyer GM, Carn SA, Tsanev VI, Oppenheimer C, Burton M (2008) Investigation into magma
320 degassing at Nyiragongo volcano, Democratic Republic of the Congo. Geochem Geophys
321 Geosys 9:Q02017. doi:10.1029/2007GC001829.

322 Sigurdsson H, Brown GM (1970) An Unusual Enstatite-Forsterite Basalt from Kolbeinsey
323 Island, North of Iceland. J petrol 11:205-220

324 Wenzel T, Baumgartner LP, Brügmann GE, Konnikov EG Kislov EV (2002) Partial Melting
325 and Assimilation of Dolomitic Xenoliths by Mafic Magma: the Ioko-Dovyren Intrusion (North
326 Baikal Region, Russia). J Petrol 43:2049-2074

327

328 **Figure captions**

329 Figure 1: BSE (Back Scattered Electron) images of olivine grains in MGR-2 (A) and AND-3
330 (B, C and D) samples. In each crystal, the dark part is pure forsterite and the grey part is Fe-
331 rich olivine plus Fe-rich oxides.

Figure 2: Forsterite content of the different parts of the analyzed grains of olivine in MGR-2 (Fig. 1A) and AND-3 (Fig. 1B,C,D), compared to the composition of olivine in other Nyiragongo lavas (Badriyo Agama, unpublished data).

Figure 3: Image processed (B) of the BSE image (A) of an olivine crystal from MGR-2 sample. The calculated surface for the green and red colours allows the determination of the different proportion of forsterite and Fe-rich areas considered as olivine, and the calculation of the composition of the initial olivine crystal (See text for explanation).

Figure 4: SiO_2 and CaO content in the 4 studied olivine grains in MGR-2 and AND-3 samples versus their forsterite content, assuming that the BSE-grey parts are olivine. The grey circles correspond to olivine analyses from other Nyiragongo lavas (Badriyo Agama, unpublished data). The green field represents olivine compositions from mafic volcanic rocks worldwide (GEOROC database). In A, the black line corresponds to the calculated composition of stoichiometric olivine. In B, the squares represent the calculated composition of the initial olivine grains shown in Fig. 1.

Figure 5: Chemical maps of an olivine crystal from sample MGR-2 obtained on the electron microprobe. The colour scale shows the level of concentration of Ca (A), Fe (B), Mg (C) and Si (D).

Figure 6: BSE image (A) and chemical maps of a small portion of an olivine crystal from MGR-2 sample obtained on the electron microprobe. The crystal is the large one shown on Fig. 1A, 3 and 5. The colour scale shows the level of concentration of Fe (B), Mg (C) and Si (D).

Figure 7: BSE image (A) and chemical maps of a small portion of an olivine crystal from AND-3 sample obtained on the electron microprobe. The crystal is the large one shown on Fig. 1B. The colour scale shows the level of concentration of Fe (B), Mg (C) and Si (D).

Table captions

Table 1 Major element composition (wt. %) of the two studied samples.

Table 2 Electron microprobe analyses of olivine in the two studied samples. D is for BSE-dark, G is for BSE-grey. Fo is the forsterite content calculated from the analyses.

Table 3 Calculation of the primary olivine composition from image processing and electron microprobe analyses. Image data columns represent the % of the two kinds of olivine in each analyzed crystal, calculated from image processing. Electron microprobe columns represent the average composition of dark and grey olivine for Fo and CaO. Primary olivine columns show the calculated composition of the primary olivine as a mixing of grey and dark olivine in proportions calculated from the images.

Table 4 Electron microprobe analyses of oxides around and inside the studied olivine crystals. Fe^{2+} and Fe^{3+} have been calculated using Ferracutti et al (2015) software.

Pure forsterite in Nyiragongo lavas: evidence for subsolidus oxidation of volcanic rocks

Innocent Badriyo Agama[1,3], Gilles Chazot[2*] and Pierre Kamgang[1]

[1]Département des Sciences de la Terre, Faculté des Sciences, Université de Yaoundé I, B.P. 812, Yaoundé, Cameroon

[2]Université de Brest (UBO), UMR 6538, Laboratoire Géosciences Océan, Institut Universitaire Européen de la Mer, place Copernic, 29280 Plouzané, France. ORCID : 0000-0002-2182-7459

[3]Observatoire Volcanologique de Goma. B.P. 484, Goma, Nord-Kivu, RDC

* Corresponding author: Gilles.Chazot@univ-brest.fr

Abstract

Some volcanic rocks from Nyiragongo volcano in the Democratic Republic of Congo contain highly oxidized olivine crystals. These olivines crystals are made of two phases, dark olivine on backscattered electron images of pure forsterite composition and grey Mg-poor areas made of olivine and iron-rich oxides. Calculation of the initial composition confirms that they are primary olivine with late separation of two different olivine compositions. Pure forsterite is enriched in SiO_2 but contains lower amounts of CaO than Fe-rich areas, in agreement with expected partitioning of these elements related to the composition of the olivine. Iron-rich oxides formed around or inside the olivine crystals during the separation process and confirm a highly oxidized environment during their evolution. We propose that this separation occurred during subsolidus recrystallization under high fo_2 conditions of the olivine crystals after cooling of the volcanic rocks. It provides evidences for circulation of iron-rich fluids or gas inducing deuteritic processes occurring in the large volcanic cone of the Nyiragongo, in relation with the presence of a shallow magma chamber connected to a large and permanent lava lake.

Article highlights

- Some volcanic rocks from Nyiragongo volcano contain oxidized olivine crystals with areas of different chemical compositions
- Primary olivine crystals separated into pure forsterite (Fo_{99}) and Fe-rich oxides

- Forsterite formation occurred during subsolidus recrystallization under highly oxidizing conditions related to H_2O-CO_2–Iron rich gas or fluid percolation

Keywords: Nyiragongo – Olivine – Forsterite- Oxidation

Declarations

Funding: World Bank

Conflict of interest: On behalf of all authors, the corresponding author states that there is no conflict of interest

Availability of data and material: Most of the data are in the tables. More data and samples are available on request.

Code availability: Not applicable

Acknowledgements

We wish to thank Jessica Langlade for her precious help during electron microprobe analyses and mapping, and Marion Jaud for processing and calculation on the chemical maps. We thank an anonymous reviewer and especially TomAndersen who provided a very interesting review which helped us for a better understanding of our samples. The World Bank is acknowledged for funding the “Projet d’Amélioration de la Capacité de la RDC à Gérer, Surveiller et réagir aux Risques Naturels dans la Région de Goma (GFDRR TF-OA162)“ of which this work is part.

Table 1

	AND-3	MGR-2
SiO_2	42.18	40.41
TiO_2	3.67	3.39
Al_2O_3	14.44	12.14
Fe_2O_3	13.35	13.10
MnO	0.21	0.20
MgO	5.95	7.92
CaO	11.73	14.67
Na_2O	3.66	2.59
K_2O	3.84	2.71
P_2O_5	0.71	0.74
LOI	0.23	0.38
Total	99.96	98.26
Mg#	46.9	54.5

Table 2

Sample	MGR-2																		
Analysis n°	28	29	30	31	32	2	3	4	5	6	7	8	9	10	11	22	23	24	25
	D	G	D	G	D	D	D	D	D	G	G	G	G	G	G	D	D	D	D
SiO_2	42.87	38.98	42.80	37.56	43.74	42.59	42.95	43.03	43.09	40.10	39.03	36.27	38.42	38.90	37.60	43.05	43.30	42.67	42.84
TiO_2	0.02	0.00	0.00	0.00	0.00	0.02	0.07	0.02	0.05	0.00	0.04	0.05	0.03	0.02	0.04	0.03	0.02	0.02	0.03
Al_2O_3	0.01	0.11	0.00	0.10	0.02	0.01	0.05	0.00	0.00	0.10	0.10	0.06	0.08	0.06	0.12	0.00	0.03	0.03	0.04
Cr_2O_3	0.00	0.07	0.00	0.07	0.00	0.00	0.00	0.00	0.00	0.04	0.07	0.07	0.04	0.00	0.08	0.02	0.00	0.00	0.00
FeO	0.67	31.56	0.69	33.40	3.90	2.58	0.71	0.64	0.71	30.86	31.40	35.55	32.65	18.25	29.95	0.38	0.35	1.71	0.79
MnO	0.14	0.25	0.20	0.20	0.34	0.20	0.14	0.17	0.19	0.17	0.23	0.18	0.19	0.21	0.18	0.11	0.23	0.37	0.28
MgO	56.80	25.57	56.51	25.05	50.46	54.13	56.21	56.53	57.04	26.68	25.91	25.33	25.33	43.23	29.26	57.51	57.11	54.86	56.71
CaO	0.05	0.83	0.12	0.91	0.36	0.98	0.02	0.14	0.09	1.01	1.11	0.95	0.77	0.58	0.95	0.03	0.00	0.95	0.32
NiO	0.24	0.02	0.23	0.05	0.18	0.29	0.19	0.25	0.23	0.10	0.11	0.05	0.08	0.12	0.11	0.01	0.00	0.00	0.05
Total	100.81	97.40	100.56	97.33	99.01	100.88	100.32	100.85	101.42	99.17	98.16	98.60	97.73	101.48	98.45	101.18	101.03	100.64	101.07
Fo	99.34	59.09	99.32	57.21	95.84	97.40	99.30	99.37	99.30	60.65	59.53	55.95	58.04	80.85	63.53	99.63	99.66	98.29	99.22

Sample	AND-3																						
Analysis n°	46	47	48	49	50	56	72	73	27	28	29	30	32	33	38	42	43	44	45	49	50	51	52
	D	D	G	G	D	D	D	D	D	D	G	G	D	G	G	D	D	G	G	G	G	G	D
SiO_2	43.21	42.84	36.31	39.68	43.28	43.33	42.57	42.62	42.83	42.99	39.06	38.04	43.02	38.70	40.27	43.03	42.33	39.96	39.75	36.54	36.71	39.77	42.86
TiO_2	0.10	0.04	0.04	0.05	0.06	0.00	0.02	0.03	0.01	0.05	0.01	0.05	0.07	0.17	0.25	0.06	0.07	0.03	0.07	0.03	0.04	0.10	0.05
Al_2O_3	0.04	0.00	0.12	0.16	0.07	0.05	0.02	0.08	0.04	0.00	0.09	0.06	0.04	0.19	0.32	0.04	0.01	0.06	0.11	0.07	0.14	0.06	0.02
Cr_2O_3	0.00	0.00	0.00	0.00	0.00	0.00	0.00	0.00	0.00	0.00	0.00	0.04	0.00	0.00	0.00	0.00	0.00	0.00	0.00	0.00	0.01	0.00	0.00
FeO	2.47	0.70	45.10	27.01	0.80	0.73	1.72	3.66	2.06	1.88	28.73	33.61	1.23	31.92	29.27	0.87	0.87	27.11	37.12	38.27	47.45	24.01	0.88
MnO	0.34	0.43	0.17	0.51	0.44	0.31	0.27	0.26	0.26	0.26	0.34	0.20	0.26	0.24	0.22	0.21	0.30	0.45	0.21	0.24	0.13	0.43	0.26
MgO	54.21	56.87	14.45	28.66	56.59	56.90	56.07	53.74	55.83	56.04	30.69	26.51	57.08	26.78	28.47	56.81	56.89	29.04	17.34	18.64	9.98	33.93	56.42
CaO	0.14	0.27	0.45	0.55	0.08	0.11	0.06	0.31	0.16	0.06	0.69	0.58	0.13	0.35	0.18	0.11	0.20	0.59	0.42	1.30	0.11	0.46	0.14
NiO	0.20	0.17	0.06	0.21	0.16	0.15	0.16	0.21	0.13	0.16	0.12	0.15	0.17	0.06	0.01	0.27	0.15	0.15	0.13	0.05	0.04	0.15	0.19
Total	100.71	101.32	96.69	96.82	101.49	101.58	100.89	100.91	101.35	101.50	99.81	99.31	101.99	98.65	99.15	101.49	100.89	97.51	95.43	95.35	94.82	99.03	100.90
Fo	97.51	99.31	36.35	65.41	99.21	99.29	98.30	96.32	97.98	98.15	65.57	58.44	98.81	59.92	63.43	99.14	99.15	65.63	45.44	46.47	27.27	71.59	99.13

Table 3

	Image data		Electron microprobe data				Primary olivine	
	% dark	% grey	Fo dark	Fo grey	CaO dark (wt.%)	CaO grey (wt.%)	Fo	CaO
MGR-2	77.5	22.5	99.3	60.0	0.10	1.00	90.5	0.30
AND-3 olivine 1	65.9	34.1	98.0	60.0	0.10	0.50	85.0	0.24
AND-3 olivine 2	69.5	30.5	99.1	65.0	0.18	0.50	88.7	0.28
AND-3 olivine 3	77.2	22.8	99.0	65.0	0.18	0.50	91.2	0.25

Table 4

	MGR2			AND3								
Analysis n°	16	17	26	31	34	35	36	37	40	41	46	48
SiO_2	0.01	0.10	0.04	0.44	0.83	0.04	0.05	0.54	0.02	0.04	0.71	1.96
Al_2O_3	1.36	0.93	1.02	1.09	3.10	0.74	5.95	0.58	0.61	5.12	1.26	1.01
TiO_2	6.53	3.92	4.31	0.52	1.99	5.07	0.50	0.11	3.82	0.22	6.87	8.97
FeO	79.52	81.47	81.58	87.39	62.96	81.13	64.08	88.38	82.83	65.18	75.81	71.73
MnO	0.81	0.55	0.53	0.07	1.31	0.54	2.09	0.04	0.37	1.84	0.95	0.87
MgO	3.20	2.19	2.26	0.45	22.31	2.78	19.83	0.91	2.12	19.82	5.65	6.16
CaO	0.10	0.08	0.20	0.07	0.14	0.16	0.09	0.03	0.05	0.12	0.27	0.54
Cr_2O_3	0.11	0.02	0.25	0.00	0.00	0.00	0.00	0.00	0.00	0.01	0.00	0.00
NiO	0.05	0.06	0.04	0.00	0.15	0.05	0.12	0.06	0.02	0.21	0.05	0.08
TOTAL	91.69	89.30	90.22	90.04	92.79	90.52	92.71	90.65	89.85	92.56	91.57	91.31
Fe^{2+}(calculated)	30.54	29.20	29.73	30.29	0.00	29.69	0.00	29.56	29.69	0.00	27.60	28.98
Fe^{3+}(calculated)	54.42	58.09	57.62	63.45	69.97	57.17	71.21	65.37	59.06	72.44	53.58	47.50

Figure 1

Click here to access/download;Figure (must NOT contain author information);Fig1.tif

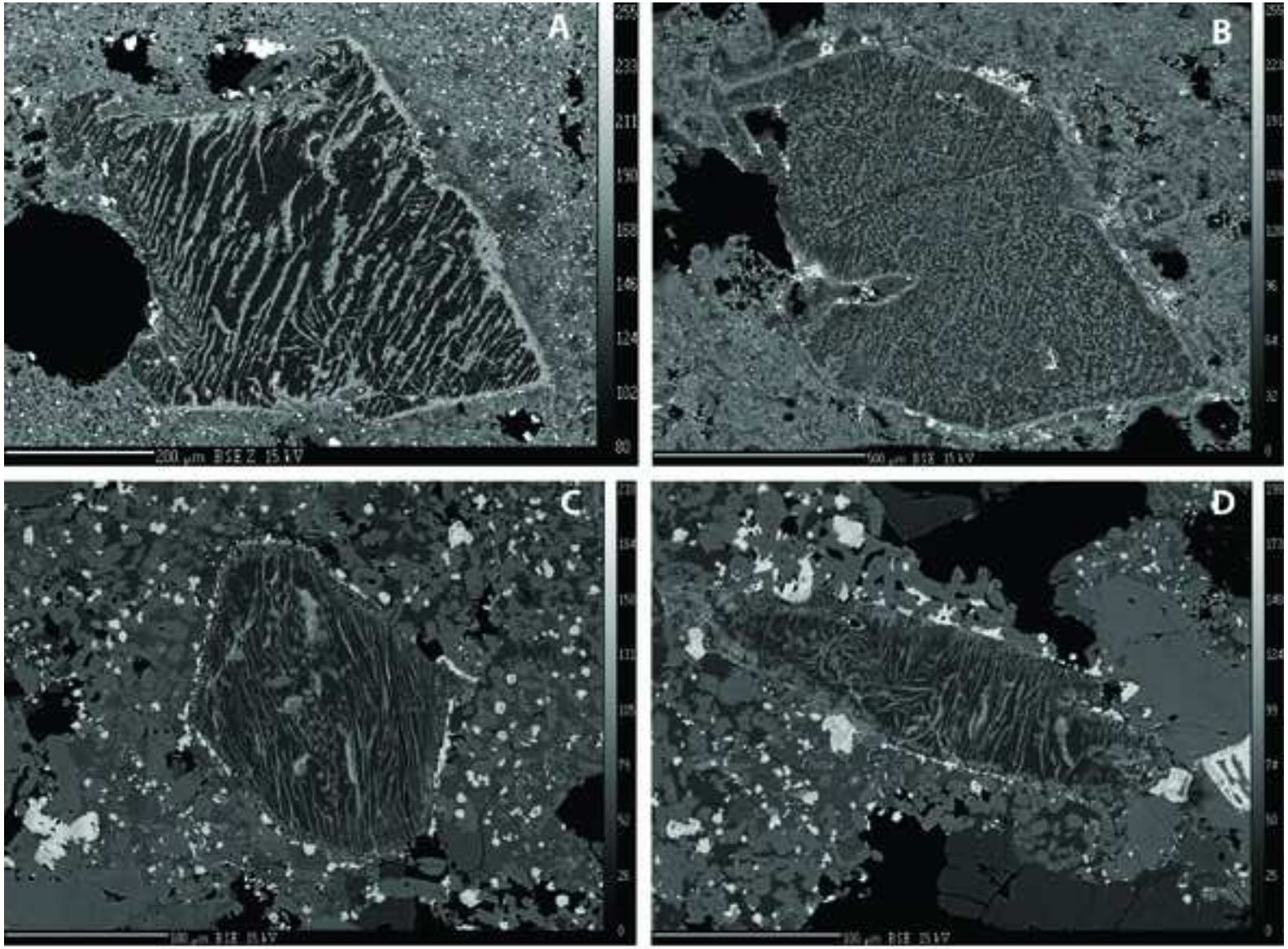

Figure 1

Figure 2

Click here to access/download;Figure (must NOT contain author information);Fig2.eps

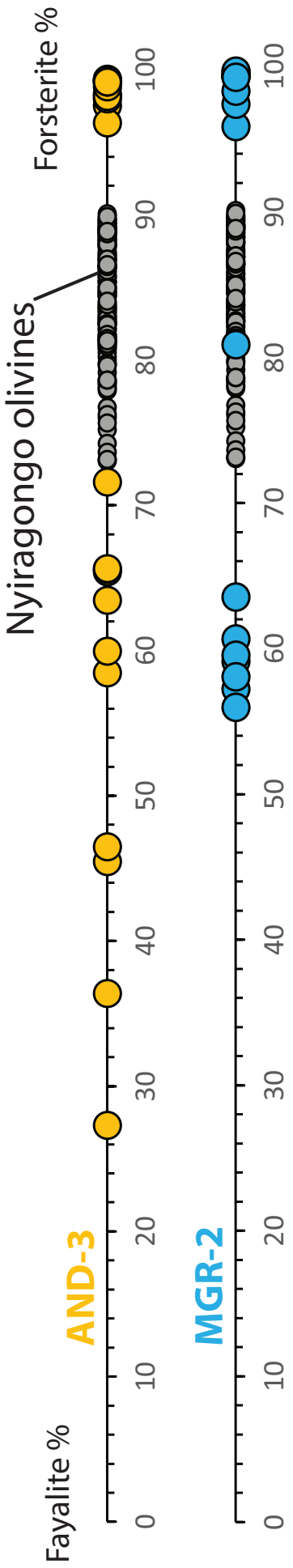

Figure 2

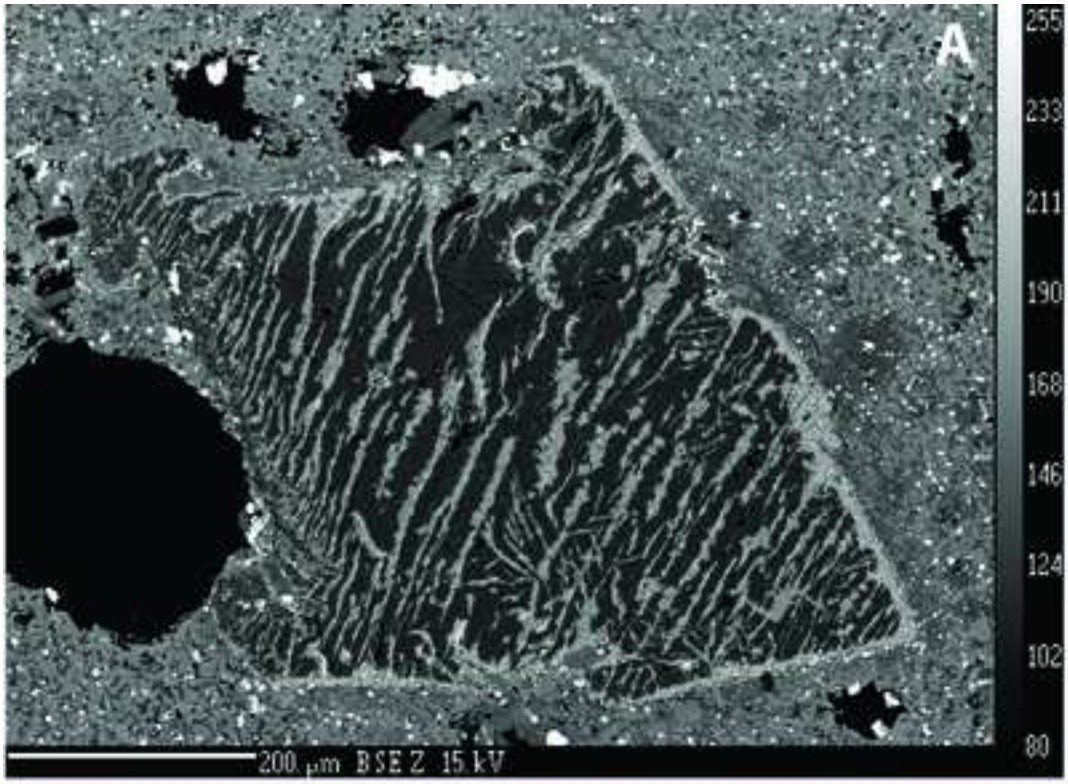

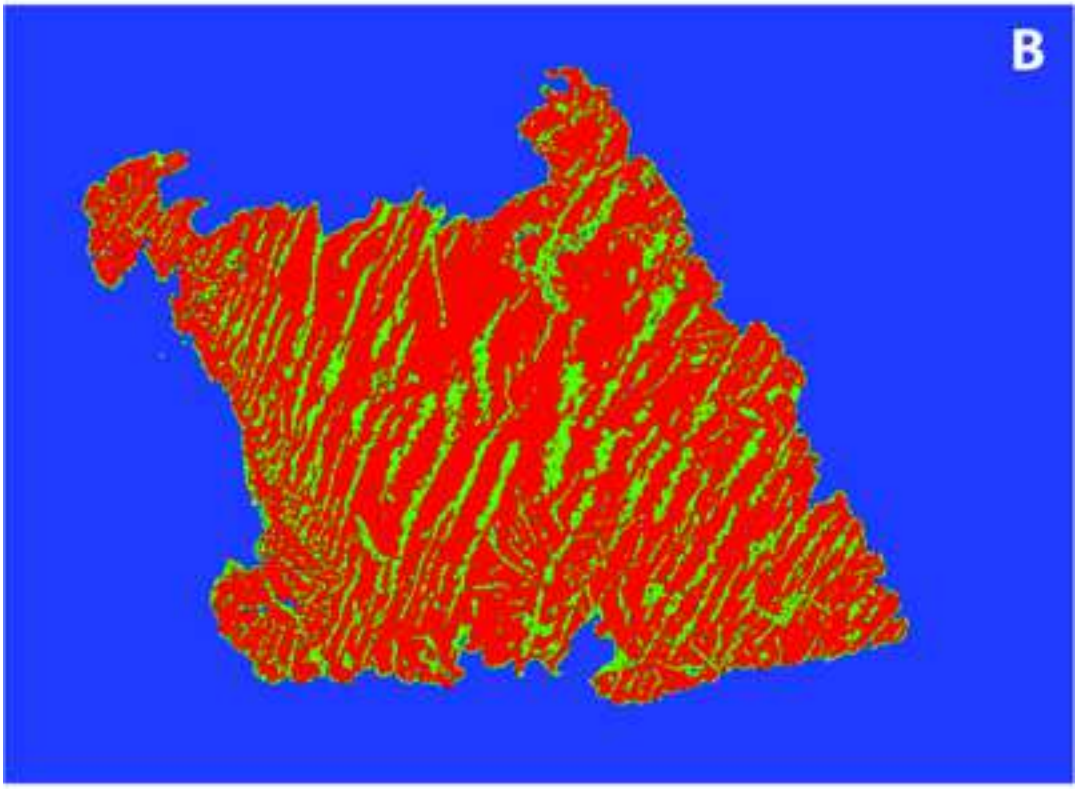

Figure 3

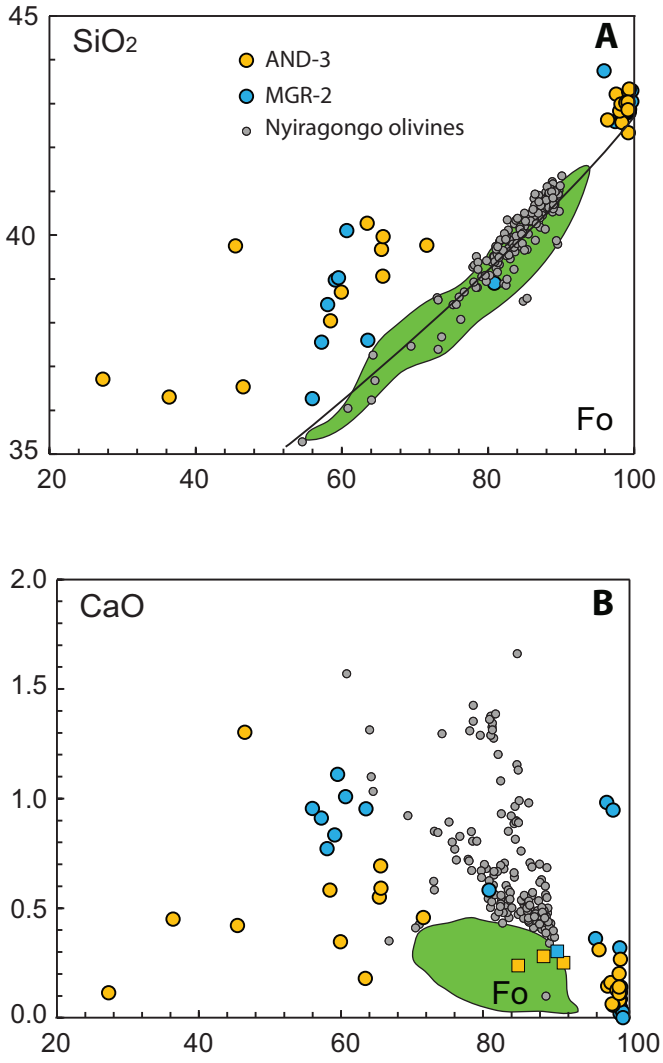

Figure 4

Figure 5

Click here to access/download;Figure (must NOT contain author information);Fig5.tif

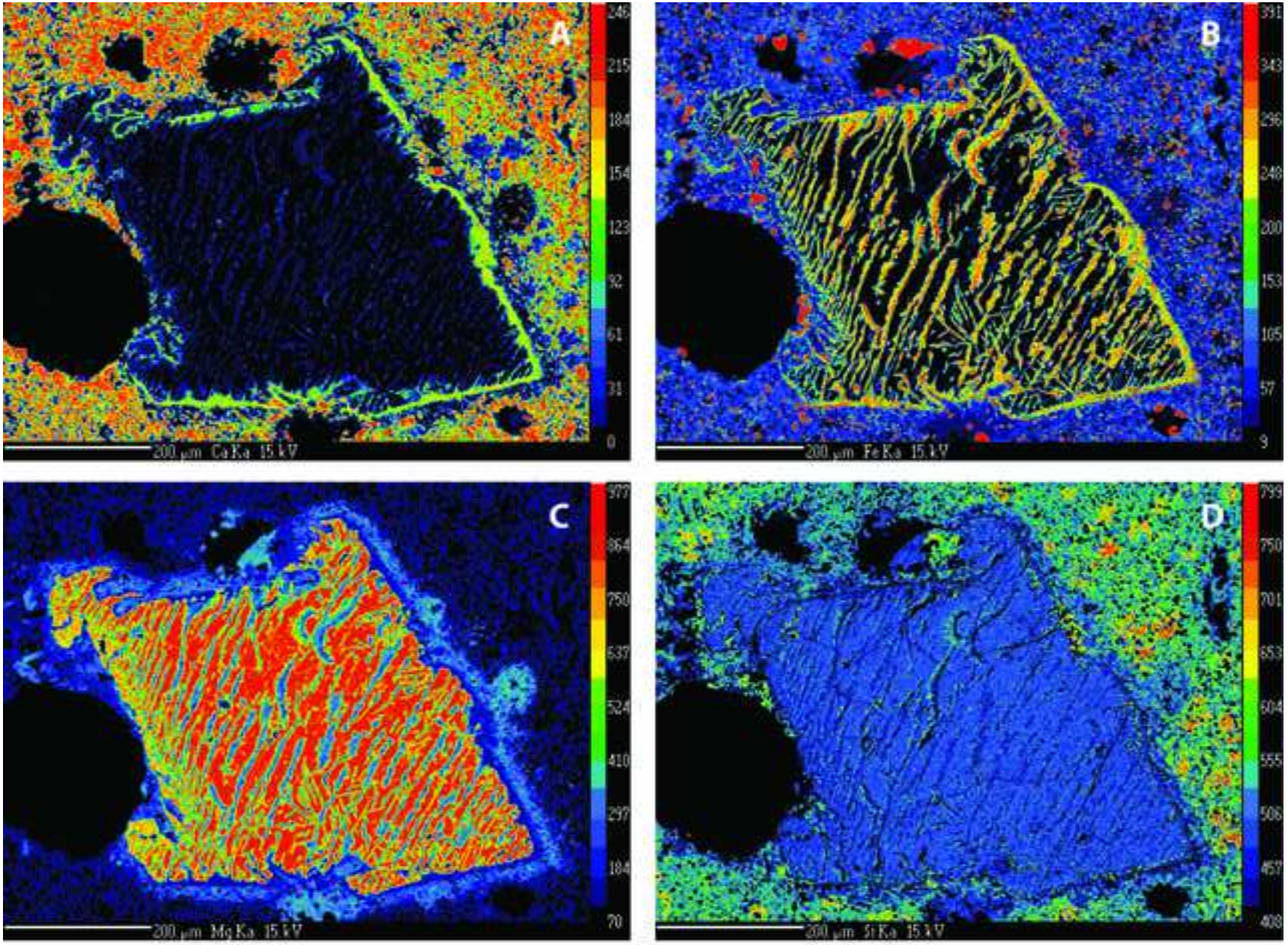

Figure 5

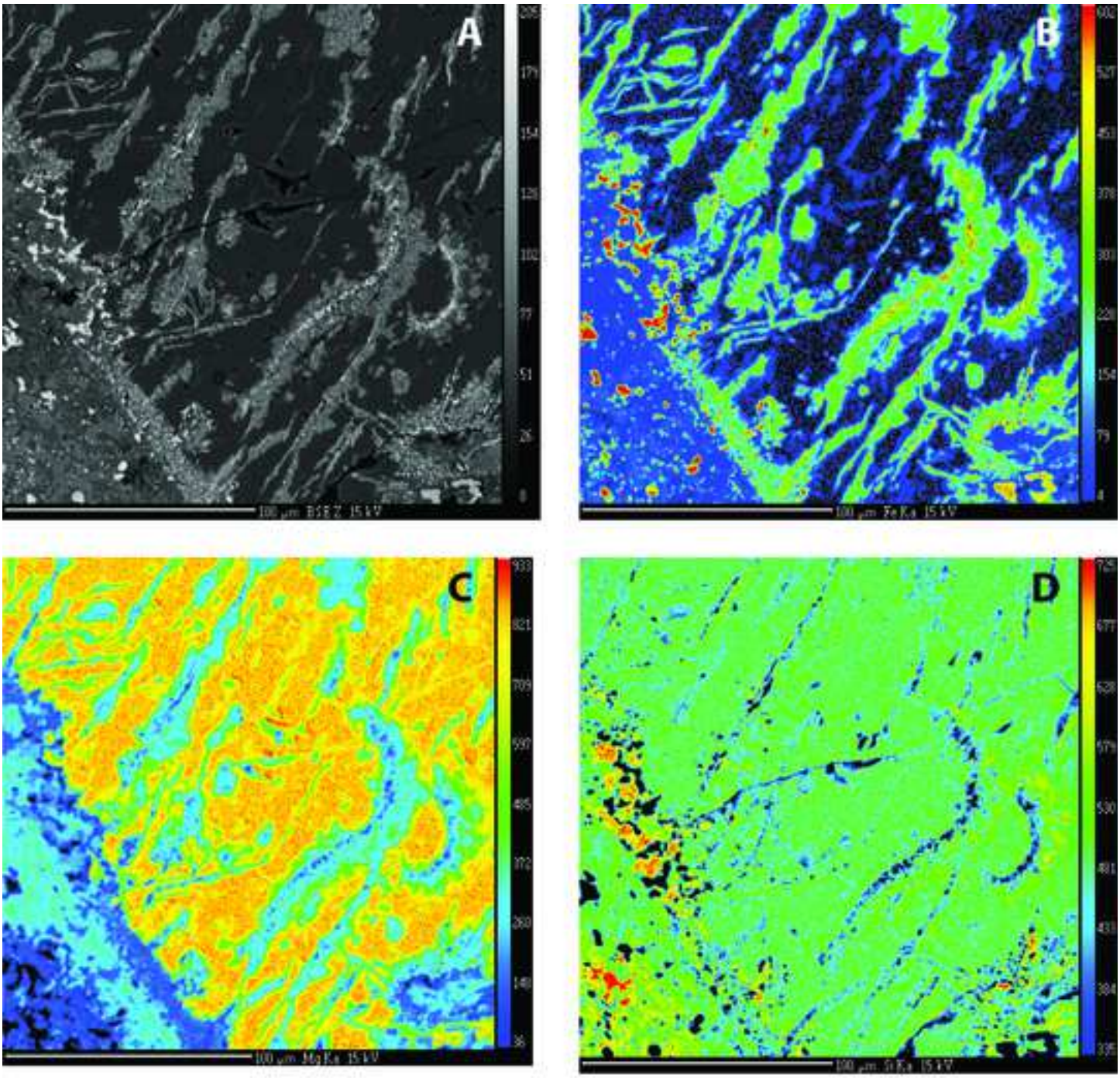

Figure 6

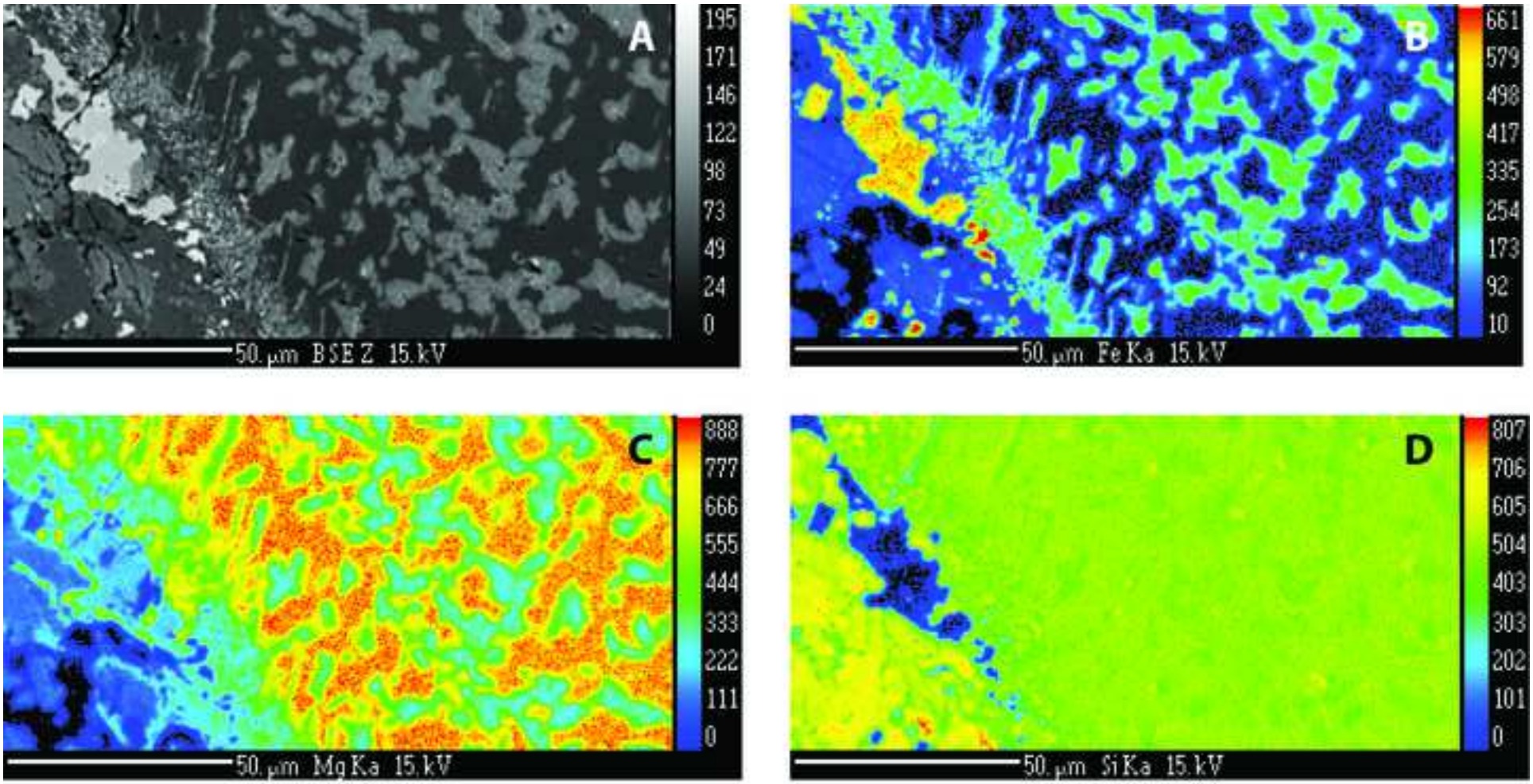

Figure 7